Diagnosing the Influence of Mesoscale Eddy Fluxes on the Deep Western Boundary Current in the 1/10° STORM/NCEP Simulation

VEIT LÜSCHOW

Max Planck Institute for Meteorology, and International Max Planck Research School on Earth System Modelling, Hamburg, Germany

JIN-SONG VON STORCH AND JOCHEM MAROTZKE

Max Planck Institute for Meteorology, Hamburg, Germany

(Manuscript received 25 May 2018, in final form 5 January 2019)

ABSTRACT

Using a 0.1° ocean model, this paper establishes a consistent picture of the interaction of mesoscale eddy density fluxes with the geostrophic deep western boundary current (DWBC) in the Atlantic between 26°N and 20°S. Above the DWBC core (the level of maximum southward flow, ~2000-m depth), the eddies flatten isopycnals and hence decrease the potential energy of the mean flow, which agrees with their interpretation and parameterization in the Gent–McWilliams framework. Below the core, even though the eddy fluxes have a weaker magnitude, they systematically steepen isopycnals and thus feed potential energy to the mean flow, which contradicts common expectations. These two vertically separated eddy regimes are found through an analysis of the eddy density flux divergence in stream-following coordinates. In addition, pathways of potential energy in terms of the Lorenz energy cycle reveal this regime shift. The twofold eddy effect on density is balanced by an overturning in the plane normal to the DWBC. Its direction is clockwise (with upwelling close to the shore and downwelling further offshore) north of the equator. In agreement with the sign change in the Coriolis parameter, the overturning changes direction to anticlockwise south of the equator. Within the domain covered in this study, except in a narrow band around the equator, this scenario is robust along the DWBC.

1. Introduction

Mesoscale eddies can contribute about 2/3 to the overall kinetic energy budget of the oceans (von Storch et al. 2012). In recent years, the increasing availability of eddy-resolving global ocean simulations (e.g., Griffies et al. 2015; von Storch et al. 2016) as well as high-resolution altimetry (e.g., Chelton et al. 2007) have substantially enhanced our knowledge of how eddies affect the large-scale ocean circulation. However, research on eddies has predominantly focused on those occurring near the surface, while deep eddies and their interaction with deep ocean currents has received little attention. Here, we address one such current, namely, the deep western boundary current (DWBC) in the Atlantic, and describe its interplay with mesoscale eddy fluxes.

The DWBC is expected to constitute the deep limb of the Atlantic meridional overturning circulation (AMOC; Fine 1995). Yet, recent observational studies question the continuous nature of the DWBC, in particular near the Grand Banks at 42°N, and stress the importance of interior pathways for North Atlantic Deep Water (NADW) toward the south (Fischer and Schott 2002; Bower et al. 2009). However, most authors agree that south of the Bahamas, the DWBC is a more or less coherent current and the primary conduit for NADW (Garzoli et al. 2015; Rhein et al. 2015; Buckley and Marshall 2016). Hence, we focus our attention on the DWBC segment between the Bahamas (26°N) and the Trinidad seamount chain (20°S) where the DWBC is expected to become less coherent (Garzoli et al. 2015). Numerous observational records exist in this DWBC segment, and several of them report strong eddy activity (Lee et al. 1996; Dengler et al. 2004; Schott et al. 2005; Garzoli et al. 2015).

Corresponding author: Veit Lüschow, veit.lueschow@mpimet.mpg.de

DOI: 10.1175/JPO-D-18-0103.1

According to the prevailing interpretation of eddy–mean flow interaction, eddies originate from baroclinic instabilities and act to release potential energy from the mean flow which is supported by the large-scale buoyancy or wind forcing (Charney 1947; Gill et al. 1974). The Gent–McWilliams (GM) parameterization of mesoscale eddies, widely used in coarse-resolution ocean models, likewise follows this notion of eddies and flattens isopycnals via an additional eddy-induced advection (Gent et al. 1995). However, several authors report huge spatial variations as well as sign changes in the so-called thickness diffusivity κ that sets the magnitude of the additional advection (e.g., Jayne and Marotzke 2002; Eden et al. 2007). Sign changes in κ imply that eddies partly behave contrary to expectations by feeding potential energy to the mean flow. In this study, we address this confusion and clarify the effect of mesoscale eddy fluxes on the mean density distribution near the DWBC. To the best of our knowledge, this issue has not been investigated in the existing literature. We use the STORM/NCEP simulation, performed with the Max Planck Institute Ocean Model (MPI-OM) at 0.1° horizontal resolution; because we expect the 0.1° model to resolve the major part of the eddy field, the GM parameterization is switched off.

We begin this paper by assessing the ability of the STORM model to represent the observed DWBC (section 2). In the same section, we provide a brief phenomenology of the simulated eddy field near the DWBC, which is less known from observations. The results section (section 3) is organized in three segments: In the first segment (section 3a), we analyze in detail the effect of the eddy density flux on the mean density. The second segment (section 3b) takes a different perspective on the same issue and investigates pathways of potential energy near the DWBC. We dedicate the third segment (section 3c) to a mean circulation in the plane normal to the DWBC that balances the effect of eddy density fluxes on mean density. Section 4 provides our conclusions.

2. An eddying DWBC in the STORM simulation

We use the global ocean model MPI-OM, forced with NCEP–NCAR Reanalysis-1 data (Kalnay et al. 1996) in the STORM configuration. It has a horizontal resolution of 0.1° near the equator. The model has 80 depth levels, with the layer thickness increasing from about 50 to 150 m over the DWBC depth range, allowing for a reasonable representation of the vertical structure of the DWBC. The simulation was run from 1948 to 2010; here, we use the last 10 years of model output. Further details on the model can be found in von Storch et al. (2012) and Li and von Storch (2013), and von Storch et al. (2016) present additional results inferred from this STORM simulation.

The STORM model represents the observed DWBC reasonably well in its meridional velocity magnitude and its lateral and vertical extension. However, the net meridional transport in our model is too low by a factor of 2. We assess the realism of the DWBC in STORM by comparison against observations from 26.5°N, where the DWBC has been covered well by observations since the late 1980s. Estimates of its time-averaged southward transport range from 11 Sv ($1\,\mathrm{Sv} \equiv 10^6\,\mathrm{m^3\,s^{-1}}$; Meinen et al. 2006) to 40 Sv (Lee et al. 1996). This large spread originates from a large DWBC variability on different time scales (standard deviation of up to 20 Sv; Bryden et al. 2005a) as well as different observational setups. In our model, the effective southward DWBC transport at 26.5°N is 13 Sv. This transport consists of a narrow and strong boundary current of 120 km width that accounts for 23 Sv *southward* flow and an adjacent *northward* recirculation of 10 Sv that extends to about 550 km offshore (Fig. 1, top). Compared to recent observational studies by Meinen et al. (2013) and Johns et al. (2008) that use the RAPID array data (e.g., Cunningham et al. 2007; Kanzow et al. 2007), the net transport in our model seems to be too low, which we think is due to too strong northward recirculations. However, we find that the lateral and vertical extension of the flow, including the sign change in the meridional velocity at about 120 km offshore and the maximum velocity in the core (about $0.2\,\mathrm{m\,s^{-1}}$; Fig. 1), match observations (Lee et al. 1996; Bryden et al. 2005a). Although STORM does not resolve the two distinct vertically separated DWBC cores, consisting of upper and lower NADW (Meinen and Garzoli 2014; Smeed et al. 2018), the DWBC core depth in our model (~2000 m) agrees with the mean depth of the two observed DWBC cores. This is in contrast to earlier modeling studies like Baehr et al. (2004), who find a too shallow DWBC in their 1/3° Family of Linked Atlantic Modeling Experiments (FLAME) model with 45 depth levels. To clarify whether the improvement in simulating the DWBC is due to higher vertical or horizontal resolution, we conduct a second STORM simulation with 40 instead of 80 depth levels and the same horizontal resolution of 0.1°. The DWBC core depth in this simulation is still about correct (not shown), indicating that accurately resolving the mesoscale is key to modeling the DWBC core at the correct depth.

We find similarly good agreement between the DWBC in STORM and observations at other latitudes, such as at 18°S (Weatherly et al. 2000), between 5° and 10°S (Schott et al. 2002) and at 25°N (Bryden et al.

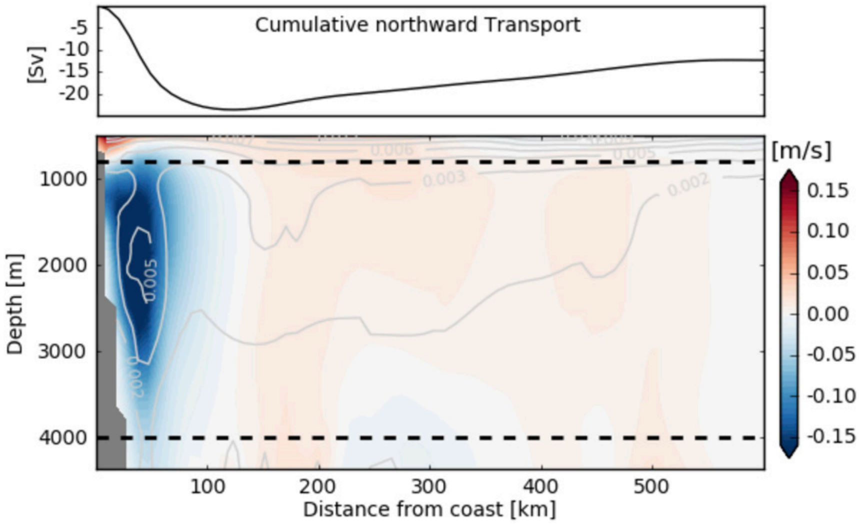

FIG. 1. (top) STORM cumulative meridional transport of NADW between 800- and 4000-m depth. The transport is computed from the western boundary eastward. (bottom) Meridional section along 26.5°N. Meridional flow in colors (positive, red northward). Gray contour lines show eddy kinetic energy ($m^2 s^{-2}$); the dashed lines define the layer of NADW, i.e., the area of DWBC transport relevant for the cumulative transport in the top panel.

2005b). Although the net transport in STORM seems to be considerably lower compared to observations, its 13 Sv southward transport accounts for 80% of the southward transport that is necessary to balance the upper-ocean northward transport at 26.5°N. We define the upper-ocean northward transport as the zonally integrated transport above 800 m, which we find is 16.4 Sv at this latitude.

Several observational studies report eddy activity near the DWBC (Lee et al. 1996; Schott et al. 2002;

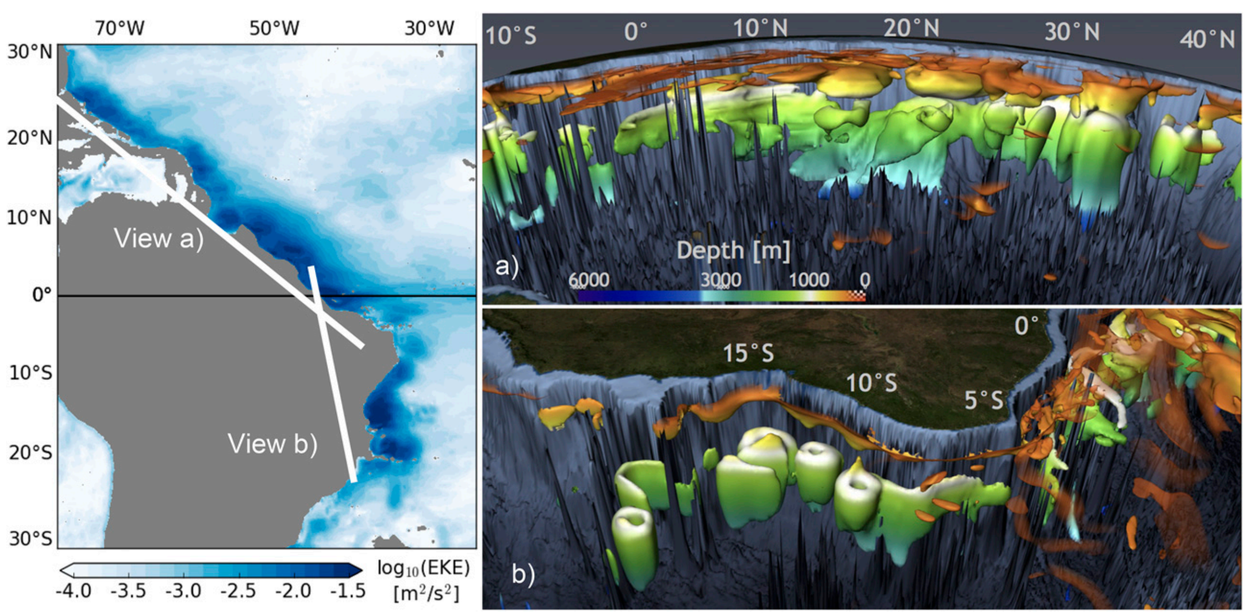

FIG. 2. (left) EKE at 1941-m depth in logarithmic color scale (blue contours). (right) 3D snapshots of the 0.2 m s^{-1} velocity magnitude contour surface. The color indicates depth, with white at 1000 m, where the DWBC begins (the color bar is nonlinear). The flow above 400 m is made transparent, because it would otherwise mask the DWBC. The angles of view of snapshots (a) and (b) are marked on the map in the left panel in white lines.

Dengler et al. 2004; Schott et al. 2005; Garzoli et al. 2015); the distribution of eddy kinetic energy (EKE) in STORM likewise shows strong eddy activity near the DWBC (Fig. 2, left, and Fig. 1, bottom). Three-dimensional snapshots of the flow field reveal strongly topographically controlled eddies, propagating alongshore southward. These eddies are nearly vertically coherent over the full depth range of the DWBC between 1000 and 4000 m (Fig. 2, right). Furthermore, their intensity, measured by the EKE, varies little with depth (Fig. 1, bottom). An interesting feature of Fig. 2 (right) is that the DWBC eddies are mostly separated from the upper-ocean flow by a layer of no motion. In agreement with Dengler et al. (2004) and Schott et al. (2005), eddies south of 8°S are particularly strong (Fig. 2b). However, also further north, the model DWBC is accompanied by strong eddy features (Fig. 2a).

3. Results

As expected for any large-scale ocean current and in accordance with DWBC observations (Kanzow et al. 2006) and other numerical simulations (Sijp et al. 2012), the DWBC in STORM is mainly geostrophic. Its deviation from geostrophy $\Delta = (|\mathbf{u} - \mathbf{u}_g|)/|\mathbf{u}_g|$, where $\mathbf{u}_g = (u_g, v_g)$ is the geostrophic velocity computed from the model pressure including a contribution from sea surface height, is everywhere lower than 10% (not shown), except near the equator and in the westernmost grid cells, which are affected by boundary friction. The geostrophic nature of the flow implies that it is predominantly controlled by density via the thermal wind relation $\partial \mathbf{u}_H/\partial z = g/(f\rho_0)\mathbf{e}_z \times \rho$, where the subscript H denotes the horizontal component of the velocity field, f is the Coriolis parameter, g is the gravitational acceleration, ρ_0 is a reference density, and $\mathbf{e}_z$ is the vertical unit vector. This suggests that the effect of mesoscale eddies on the DWBC can best be understood by analyzing how the eddies affect density through eddy density fluxes. Nevertheless, the evolution of density and momentum is coupled, and hence, eddy momentum fluxes (Reynolds stresses) cannot be disregarded completely. We address eddy momentum fluxes at the end of the results section.

According to the prevailing interpretation of their effect on density, eddies release potential energy from the mean flow by flattening isopycnals through an eddy-induced advection (e.g., Gent et al. 1995). However, Jayne and Marotzke (2002) and Eden et al. (2007) diagnose the thickness diffusivity κ, which sets the strength of this advection, in their models and report huge spatial variability and *sign changes*

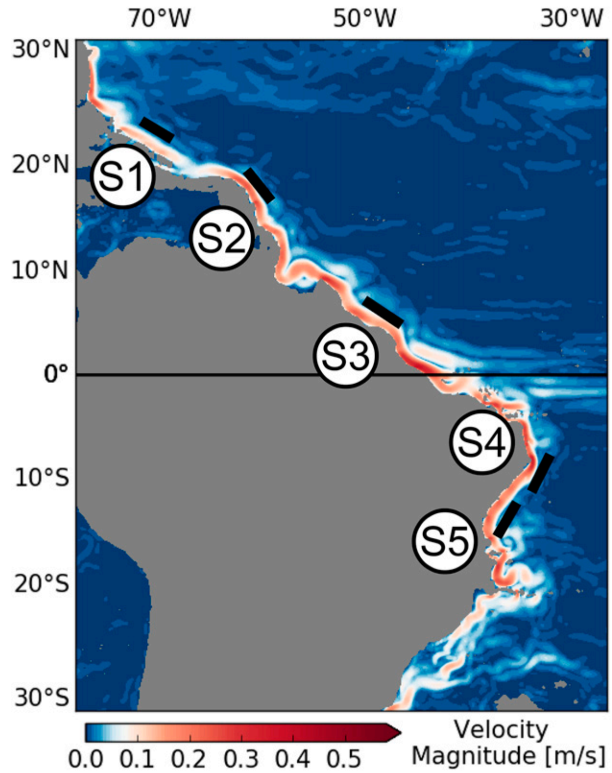

FIG. 3. Mean-flow velocity magnitude $|\overline{\mathbf{u}}|$ at 1941-m depth (nonlinear color scale). The black bars depict the five DWBC segments (S1–S5) that we analyze in this study.

herein. This would imply that eddies partly steepen isopycnals.

In the first results section, we clarify the effect of eddy density fluxes on the shape of the isopycnals near the DWBC. Subsequently, we consider the problem from an energy pathways perspective and investigate the conversion from mean to eddy potential energy. Then, we address the reaction of the mean flow to the eddies' effect.

a. The effect of eddy density flux on mean density

The evolution of mean potential density ρ can be described by the equation,

$$\frac{\partial \overline{\rho}}{\partial t} + \overline{\mathbf{u}} \cdot \nabla \overline{\rho} = -\nabla \cdot (\overline{\mathbf{u}'\rho'}) + Q, \tag{1}$$

where the total velocity $\mathbf{u} = \overline{\mathbf{u}} + \mathbf{u}'$ and potential density $\rho = \overline{\rho} + \rho'$ are each decomposed into a temporal mean (overbar) and a fluctuating (prime) component. In the remainder of this paper, density ρ always refers to potential density. The term $\overline{\mathbf{u}'\rho'}$ is the resolved eddy density flux, and Q denotes unresolved and hence parameterized diabatic mixing and nonlinear effects

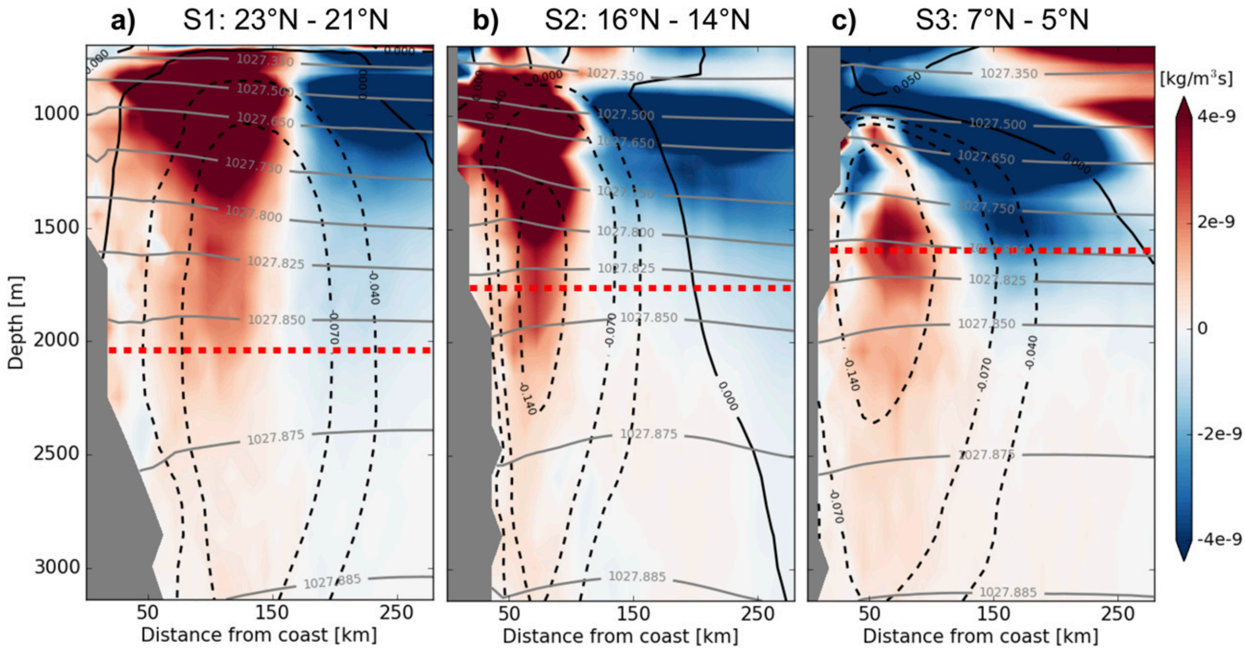

FIG. 4. Pseudozonal sections of the along-stream average of the EDFD $\nabla\cdot(\overline{\mathbf{u}'\rho'})$ (colors), surface-referenced mean potential density $\overline{\sigma}_0$ (gray contour lines), and along-streamflow $\mathbf{u}_{||}$ (black contour lines, dashed southward) (a) between 23° and 21°N (S1), (b) between 16° and 14°N (S2), and (c) between 7° and 5°N (S3). In this perspective, the DWBC flows out of the paper plane toward the reader. A positive (red) EDFD decreases and a negative (blue) EDFD increases density [note the minus sign in front of $\nabla\cdot(\overline{\mathbf{u}'\rho'})$ in Eq. (1)]. The red dashed line marks the DWBC core depth, defined as the level at which the maximum southward velocity occurs.

on density, such as cabbeling and thermobaricity. Furthermore, we expect $\partial\overline{\rho}/\partial t$ to be small, because $\overline{\rho}$ is a time-averaged quantity. In section 3c, we show that the main balance in Eq. (1) is between the eddy density flux divergence (EDFD) and the mean advection of mean potential density $\overline{\mathbf{u}}\cdot\nabla\overline{\rho}$. Therefore, we expect the EDFD $\nabla\cdot(\overline{\mathbf{u}'\rho'})$ to be a major control for the shape of the mean isopycnals and hence for the geostrophic DWBC.

We diagnose the eddy density flux via $\overline{\mathbf{u}'\rho'} = \overline{\mathbf{u}\rho} - \overline{\mathbf{u}}\,\overline{\rho}$, where the overbar represents an average over the 10 years of data used in this study. Computed this way, $\overline{\mathbf{u}'\rho'}$ contains not only fluctuations on eddy time scales, but on all time scales from the numeric time step up to the averaging period of 10 years. However, von Storch et al. (2016) compared various eddy fluxes computed from monthly mean and from 30-yr mean data and found that they do not differ significantly. Hence, we assume that $\overline{\mathbf{u}'\rho'}$ predominantly contains fluctuations due to eddies, that is, eddy fluxes.

Previous studies dealing with the effect of eddies on density analyzed eddy diffusivities that were computed from the *raw* eddy flux $\overline{\mathbf{u}'\rho'}$ in the GM framework (Jayne and Marotzke 2002; Eden et al. 2007). Yet, the raw flux contains a dynamically irrelevant rotational component, which possibly masks the effective impact of the eddies on density to an unknown extent (Marshall and Shutts 1981; Fox-Kemper et al. 2003; Eden et al. 2007). In contrast to that, we analyze the divergence of the flux and thus automatically remove the rotational part and circumvent this ambiguity. The EDFD can be interpreted in combination with the inclination of the mean isopycnals in order to assess if the eddies locally flatten or steepen isopycnals, that is, if they release potential energy from or feed potential energy to the mean flow (Treguier 1999).

The DWBC often does not flow strictly in the meridional direction but is locally aligned with the shoreline (see Fig. 3). To obtain a unified picture of the DWBC dynamics, we conduct our analysis in stream-following coordinates, where one axis points in the along-stream direction ($x_{||}$) and one normal to it ($x_{\perp}$). The velocity field $\mathbf{u}$ is rotated accordingly, and its horizontal components will be referred to as along-stream velocity $u_{||}$ and across-stream velocity $u_{\perp}$. We average all quantities of interest along the along-stream axis within each of the five DWBC segments (S1–S5) shown in Fig. 3. Every segment spans about 2° in latitude, which corresponds to roughly 220 km. By averaging segment-wise, we can improve the signal-to-noise ratio of the data and at the same time preserve potential spatial heterogeneity of the eddy–mean flow interaction in the along-stream direction of the DWBC.

Figure 4 shows pseudozonal sections of the three segments located in the Northern Hemisphere (S1–S3 in Fig. 3). Pseudozonal means that the x axis runs normal to the DWBC and the shoreline toward the open ocean. In all three segments S1–S3, above the DWBC core (~1800 m), the isopycnals (gray contour lines) are inclined upward toward the shore; below the core, they are inclined downward toward the shore. The thermal wind balance provides an explanation for this change in the isopycnic inclination, because at the same depth, the vertical shear of velocity changes sign (southward flow increasing with depth above and decreasing below the core). We present a simplified picture of this scenario in Fig. 5.

The EDFD $\nabla \cdot (\overline{\mathbf{u}'\rho'})$ (colors in Fig. 4) peaks in the upper part of the DWBC between about 800- and 1500-m depth. This is due to a local maximum in the density variance $\overline{\rho'^2}$ (not shown) and not due to stronger eddy activity. The latter is nearly constant with depth along the DWBC (see Fig. 1, bottom, for the EKE at 26°N and also the vertically coherent eddies in Fig. 2). The magnitude of the EDFD decreases with depth in all segments shown in Fig. 4, yet its sign does not change with depth. Hence, eddies decrease density (positive EDFD) close to the shore, whereas they increase density (negative EDFD) further offshore throughout the whole water column. An increase in density pushes an isopycnal upward; a decrease pushes it downward. This suggests that eddies flatten the isopycnals above the DWBC core and steepen them below. We sketch this scenario in Fig. 5, where the density increase and decrease are each visualized through upward and downward arrows, respectively.

In the two segments south of the equator (S4 and S5 in Fig. 3), eddies mainly increase density (negative EDFD) close to the shore and decrease density (positive EDFD) further offshore (Figs. 6a,b). This is the opposite of what we observe in the northern segments. However, the inclination of the isopycnals is likewise reversed due to a sign change of the Coriolis parameter at the equator. Above the DWBC core, isopycnals are inclined downward toward the shore and upward below. Thus, the net effect of eddies on the isopycnic tilt is the same in the north and in the south: eddies flatten isopycnals above the core and steepen them below. Again, we visualize the interplay between the geostrophic DWBC, the isopycnals, and the EDFD in the Southern Hemisphere in Fig. 6c.

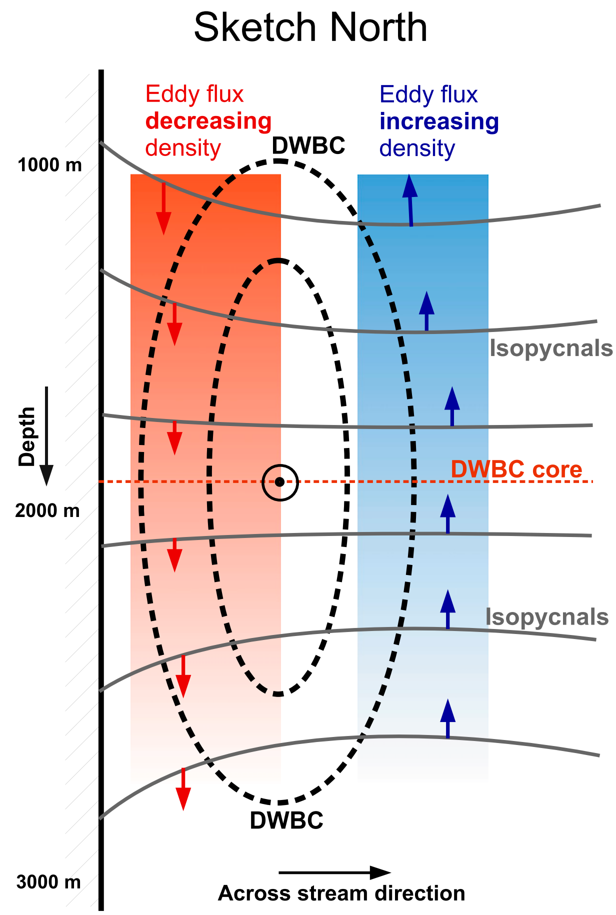

FIG. 5. Sketch of Fig. 4 that shows the EDFD (colors) and its relation to the isopycnals (gray contour lines) and along-stream velocity (black contour lines, dashed southward). North of the equator, the EDFD decreases density close to the shore (red patches here and in Fig. 4) and increases density further offshore (blue patches here and in Fig. 4). A decrease of density causes a downward shift of the isopycnals (red arrows), whereas an increase causes an upward shift (blue arrows). Again, the red dashed line marks the DWBC core depth.

b. *An energy pathways perspective on the DWBC–eddy interaction*

As already mentioned, mesoscale eddies are generally expected to extract potential energy from the mean flow and are commonly represented by a GM parameterization, either with a spatially uniform or varying thickness diffusivity κ. The rationale behind this parameterization is reflected in the assumption that in the ocean, energy is introduced through ocean–atmosphere interactions on large scales before being transferred to smaller scales and finally dissipated. The *Lorenz energy cycle* provides a quantitative description for each of the four processes involved in this energy pathway (Lorenz 1955). In the context

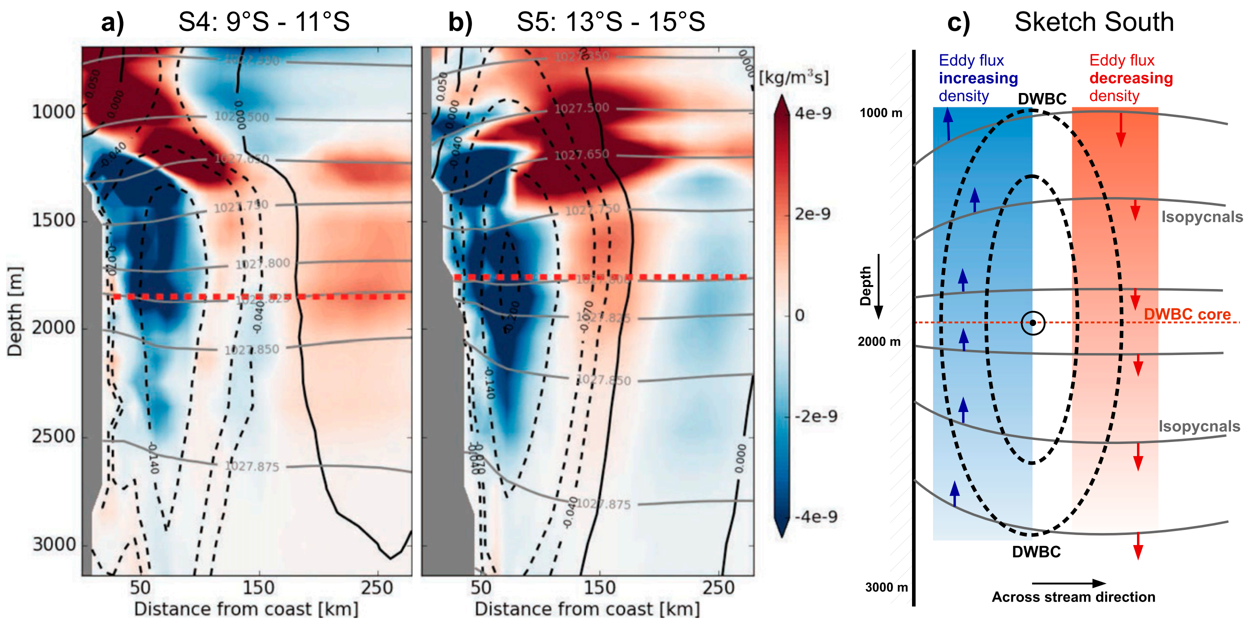

FIG. 6. Along-stream average of EDFD $\nabla \cdot (\overline{\mathbf{u}'\rho'})$ (colors), surface-referenced mean potential density $\overline{\sigma}_0$ (gray contour lines), and along-streamflow $\mathbf{u}_{||}$ (black contour lines, dashed southward) (a) between 9° and 11°S (S4) and (b) between 13° and 15°S (S5). (c) A sketch similar to Fig. 5, but for the Southern Hemisphere. The red dashed line marks the DWBC core depth.

of this study, the conversion from mean potential energy P_m to eddy potential energy P_e is relevant. A GM-like parameterization transfers potential energy exclusively from P_m to P_e. In the following, we analyze the respective conversion term in each of the five segments S1–S5 (see Fig. 3) along the DWBC in detail. For this purpose, we refer to the local conversion rate

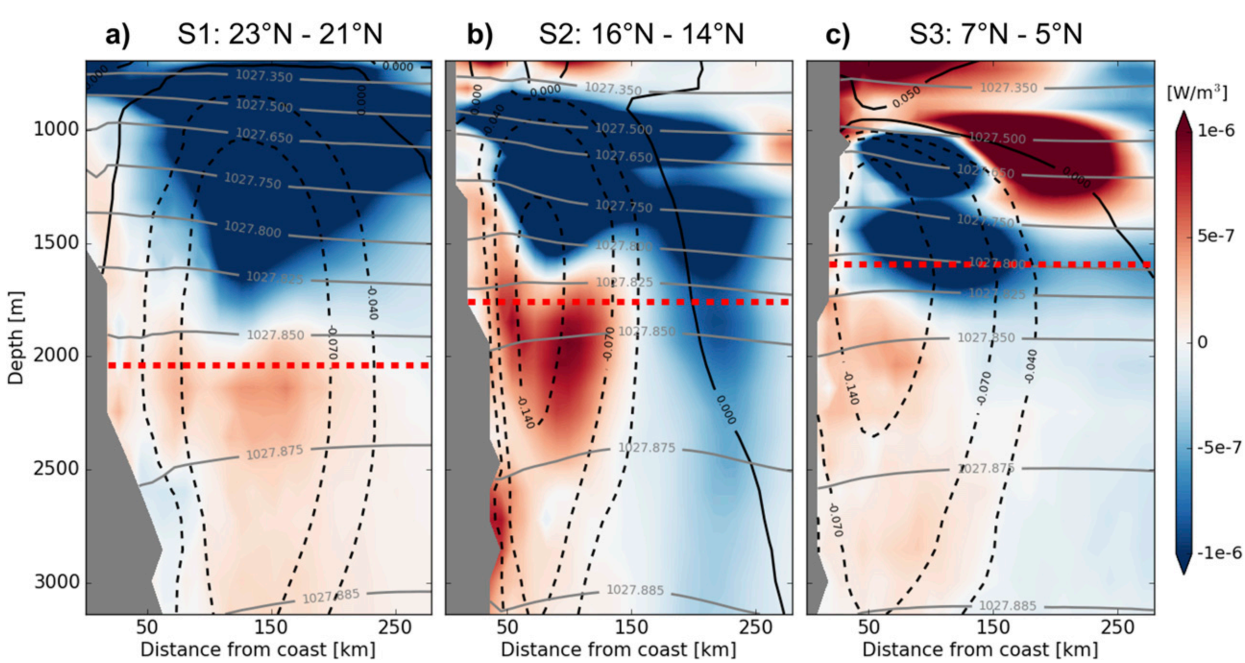

FIG. 7. Along-stream average of the conversion from eddy potential energy P_e to mean potential energy P_m $\tilde{C}(P_e, P_m)$ (colors), surface-referenced mean potential density $\overline{\sigma}_0$ (gray contour lines), and along-streamflow $\mathbf{u}_{||}$ (black contour lines, dashed southward) (a) between 23° and 21°N (S1), (b) between 16° and 14°N (S2), and (c) between 7° and 5°N (S3). A positive (red) $\tilde{C}(P_e, P_m)$ indicates a conversion $P_e \rightarrow P_m$. The red dashed line marks the DWBC core depth.

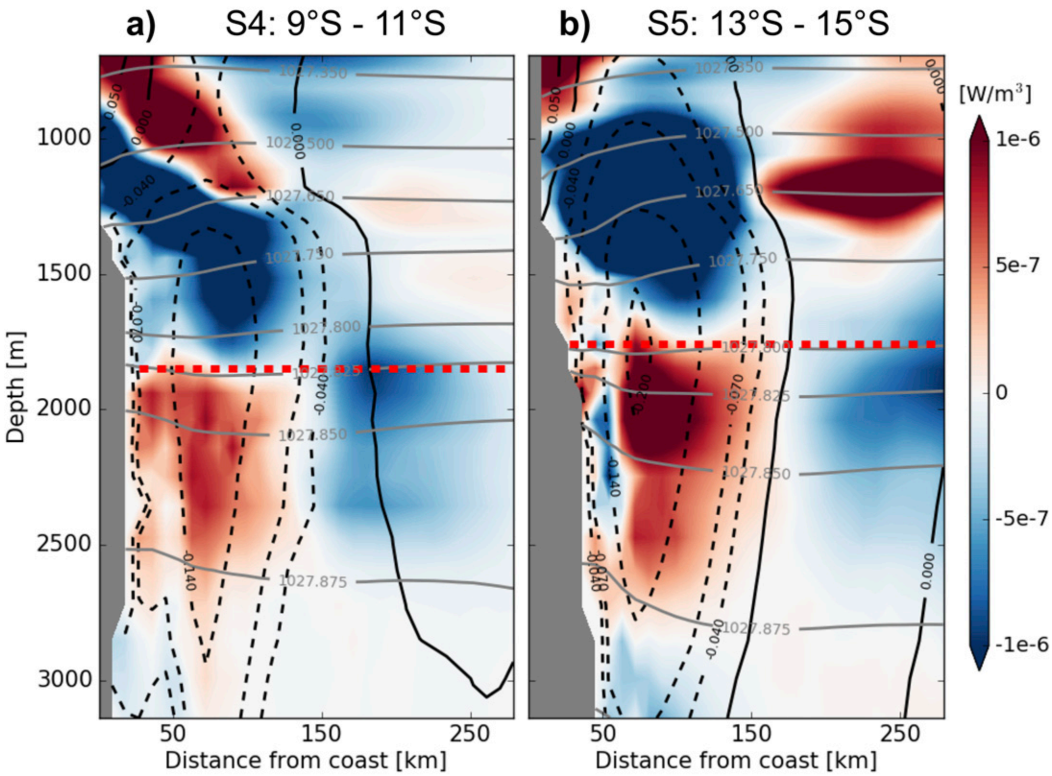

FIG. 8. Along-stream average of the conversion from eddy potential energy P_e to mean potential energy P_m $\tilde{C}(P_e, P_m)$ (colors), surface-referenced mean potential density $\overline{\sigma}_0$ (gray contour lines), and along-streamflow $\mathbf{u}_{\|}$ (black contour lines, dashed southward) (a) between 9° and 11°S (S4) and (b) between 13° and 15°S (S5). The red dashed line marks the DWBC core depth.

$$c(P_e, P_m) = \frac{g}{n_0}\overline{\mathbf{u}'_H\rho'}\cdot\nabla_H\overline{\rho}, \qquad (2)$$

which emerges from the quasigeostrophic approximation of the available potential energy equation (von Storch et al. 2012). The subscript H denotes the horizontal components of the velocity $\mathbf{u}'$ and the differential operator ∇, n_0 is the vertical gradient of the mean potential density averaged over the area of the respective segment. The conversion term $c(P_e, P_m)$ from Eq. (2) contains the horizontal components of the previously mentioned *raw* eddy flux $\overline{\mathbf{u}'\rho'}$ and thus a contribution from the dynamically irrelevant rotational part of $\overline{\mathbf{u}'\rho'}$. Marshall and Shutts (1981) identified the rotational contribution $(\overline{\mathbf{u}'_H\rho'})_R$ of $(\overline{\mathbf{u}'_H\rho'})$ in the eddy variance budget as the advection of eddy variance by the mean flow, $(\overline{\mathbf{u}'_H\rho'})_R\cdot\nabla_H\overline{\rho} = -\overline{\mathbf{u}}_H\cdot\nabla_H(\overline{\rho'^2}/2)$. When taking the along-stream average of the conversion $\tilde{C}(P_e, P_m) = 1/L\int_L c(P_e, P_m)\,dl$, where L denotes the along-stream segment length and assuming the along-stream homogeneity of the flow, only the across-stream component $-\overline{u}_\perp\partial/\partial x_\perp(\overline{\rho'^2}/2)$ of $\overline{\mathbf{u}}_H\cdot\nabla_H(\overline{\rho'^2}/2)$ remains, which should be small compared to the divergent part in the along-stream average. Griesel et al. (2014) use a similar along-stream averaging approach to minimize rotational eddy fluxes in estimates of isopycnal diffusivities. By the averaging procedure we expect $\tilde{C}(P_e, P_m)$ to contain predominantly the contribution from the divergent part of the eddy density flux $\overline{\mathbf{u}'\rho'}$. The fact that $\tilde{C}(P_e, P_m)$ agrees qualitatively well with the conversion from eddy potential energy to eddy kinetic energy $\tilde{C}(P_e, K_e) = 1/L\int_L g\overline{w'\rho'}$ (not shown) supports our assumption that $\tilde{C}(P_e, P_m)$ is a meaningful quantity (Eden et al. 2007).

In agreement with the maximum of the EDFD between 800 and 1500 m mentioned above, the overall magnitude of energy conversion likewise decreases with depth. Apart from that, we discern two distinct vertically separated regimes of potential energy conversion in the northern (Fig. 7) as well as in the Southern Hemisphere (Fig. 8): *above* the DWBC core (~1800 m), eddies transfer potential energy mainly from the mean to the eddy compartment [negative $\tilde{C}(P_e, P_m)$ in Figs. 7 and 8]. *Below* the core, eddies transfer potential energy mainly in the opposite direction from the eddy to the mean compartment [positive $\tilde{C}(P_e, P_m)$ in Figs. 7 and 8].

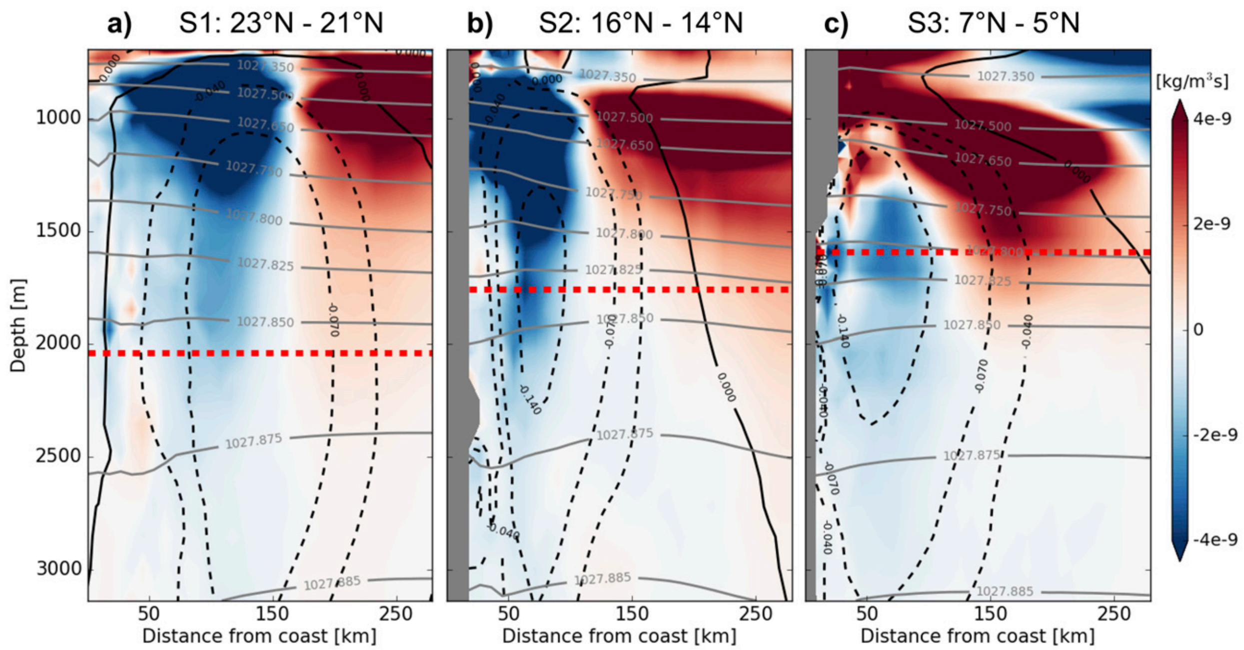

FIG. 9. Advection of mean potential density by the mean flow $\overline{\mathbf{u}} \cdot \nabla \overline{\rho}$ (colors), surface-referenced mean potential density $\overline{\sigma}_0$ (gray contour lines), and along-streamflow $\mathbf{u}_{\|}$ (black contour lines, dashed southward) for the three segments north of the equator (a) between 23° and 21°N (S1), (b) between 16° and 14°N (S2), and (c) between 7° and 5°N (S3). The red dashed line marks the DWBC core depth.

Segments S3–S5 contain exceptions in the form of smaller patches of positive conversion $\tilde{C}(P_e, P_m)$ ($P_e \rightarrow P_m$) above (S3–S5) and eastward (S3, S5) of the DWBC that we do not discuss here. However, the two conversion regimes separated at the DWBC core depth support the conclusion drawn from the analysis of the EDFD in the previous section: mesoscale eddies have a twofold effect on the mean density near the DWBC. Above the DWBC core, eddies release potential energy from the mean flow (they flatten isopycnals) and thus behave according to the GM interpretation. By contrast, below the DWBC core, they feed potential energy to the mean flow (they steepen isopycnals).

c. Mean flow balancing the effect of eddies

In our model, the budget of mean density, Eq. (1), is mainly a balance between the mean advection of mean density and the EDFD, $\overline{\mathbf{u}} \cdot \nabla \overline{\rho} \approx -\nabla \cdot (\overline{\mathbf{u}'\rho'})$. The term $\overline{\mathbf{u}} \cdot \nabla \overline{\rho}$, shown in Figs. 9 and 10 for the segments S1–S5, closely resembles the EDFD shown in Figs. 4 and 6 (with opposite sign). The residual $\overline{\mathbf{u}} \cdot \nabla \overline{\rho} + \nabla \cdot (\overline{\mathbf{u}'\rho'})$ is about one order of magnitude smaller than the two individual terms (not shown). This indicates that in our model, diabatic mixing and nonlinear effects on density such as cabbeling and thermobaricity [Q in Eq. (1)] are of minor importance near the DWBC compared to the EDFD and the density advection by the mean flow $\overline{\mathbf{u}}$. After describing the effect of the eddy fluxes in the two previous sections, we now go one step further and investigate the structure of the eddy-balancing mean flow $\overline{\mathbf{u}}$.

Within each of the DWBC segments S1–S5 shown in Fig. 3, we assume the along-streamflow to be coherent, that is, we assume the along-stream gradient of the along-stream velocity $\partial \overline{u}_{\|}/\partial x_{\|}$ to be small. Hence, the incompressibility condition, written in the along-stream/across-stream coordinate system, reduces to

$$\frac{\partial \overline{u}_{\perp}}{\partial x_{\perp}} + \frac{\partial \overline{w}}{\partial z} = 0. \tag{3}$$

Based on Eq. (3), we introduce a *pseudo-zonal overturning streamfunction*

$$\tilde{\psi}(x_{\perp}, z) = \int_0^{x_{\perp}} \tilde{\overline{w}}(x_{\perp}, z)\, dx_{\perp}^*, \tag{4}$$

which describes the time-mean flow in the plane normal to the DWBC. The tilde indicates a segment-wise along-stream average of the time-averaged vertical velocity $\overline{w}$; hence, the streamfunction ψ is also a segment-averaged quantity $\tilde{\psi}$. It has units of meters squared per second ($\mathrm{m^2\,s^{-1}}$) and describes the pseudozonal overturning per 1 m of shoreline.

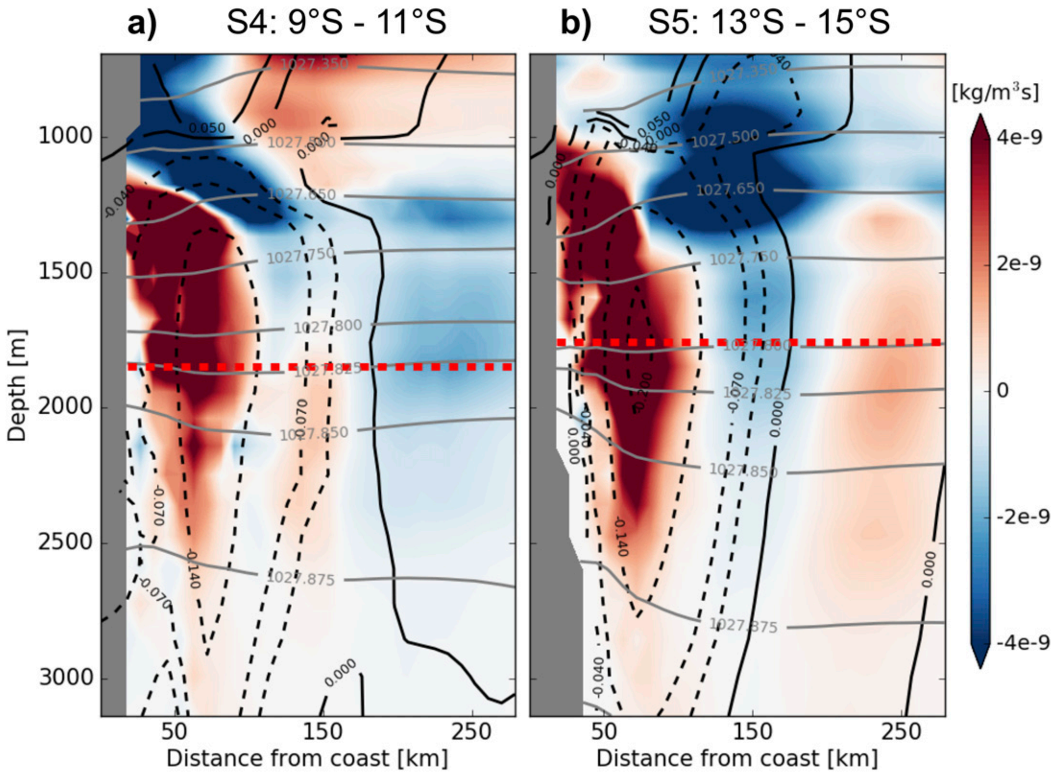

FIG. 10. Advection of mean potential density by the mean flow $\overline{\mathbf{u}} \cdot \nabla\overline{\rho}$ (colors), surface-referenced mean potential density $\overline{\sigma}_0$ (gray contour lines), and along-streamflow $\mathbf{u}_{||}$ (black contour lines, dashed southward) for the two segments south of the equator (a) between 9° and 11°S (S4) and (b) between 13° and 15°S (S5). The red dashed line marks the DWBC core depth.

The three segments in the Northern Hemisphere S1–S3 shown in Fig. 11 all show a dominant clockwise overturning cell in the plane normal to the DWBC (positive $\tilde{\psi}$). The precise shape and depth of each of these cells is different. Whereas in S1 (Fig. 11a), the overturning cell is centered at the DWBC core depth (~2000 m), the cell center and the DWBC core depth diverge when approaching the equator. Compared to S1, the DWBC core moves upward in S2 (Fig. 11b) and S3 (Fig. 11c). At the same time, the overturning cell moves downward. Nevertheless, in all segments S1–S3, the upwelling close to the shore has an effect precisely opposite to that of the EDFD described above: isopycnals are flattened below the DWBC core and steepened above. In accordance with the sign change in f and the related change in the isopycnic tilt, the pseudozonal overturning changes its direction in the Southern Hemisphere. Segments S4 and S5 each reveal a dominant anticlockwise overturning (negative $\tilde{\psi}$ in Fig. 12) normal to the DWBC, with downwelling close to the shore and upwelling further offshore. Similar to the Northern Hemisphere, the overturning cell depth and the DWBC core depth match at high latitudes in S5 (Fig. 12b), whereas the overturning cell lies deeper than the DWBC core close to the equator in S4 (Fig. 12a). However, the downwelling close to the shore flattens isopycnals below the DWBC core and steepens them above. The interaction between the overturning and the EDFD is thus the same in both hemispheres, albeit antisymmetric due to the sign change in f.

Using an eddy-resolving version of the Los Alamos Parallel Ocean Program (POP) model, Li et al. (2016) find a similar overturning normal to the mean flow in distinct segments of the Antarctic circumpolar current (ACC) and relate that overturning to the horizontal convergence of eddy momentum fluxes. In the following, we assess the potential role of eddy momentum fluxes for the overturning normal to the DWBC. The quasigeostrophic form of the along-stream-averaged along-stream momentum balance reads

$$\frac{\partial \overline{u}_{\|}}{\partial t} - f\overline{u}_{\perp} = -\frac{\partial(\overline{u'_{\perp}u'_{\|}})}{\partial x_{\perp}} + \mathscr{F}, \tag{5}$$

where $\mathscr{F}$ denotes frictional forces (Vallis 2017). We assume the first term on the left-hand side to be small

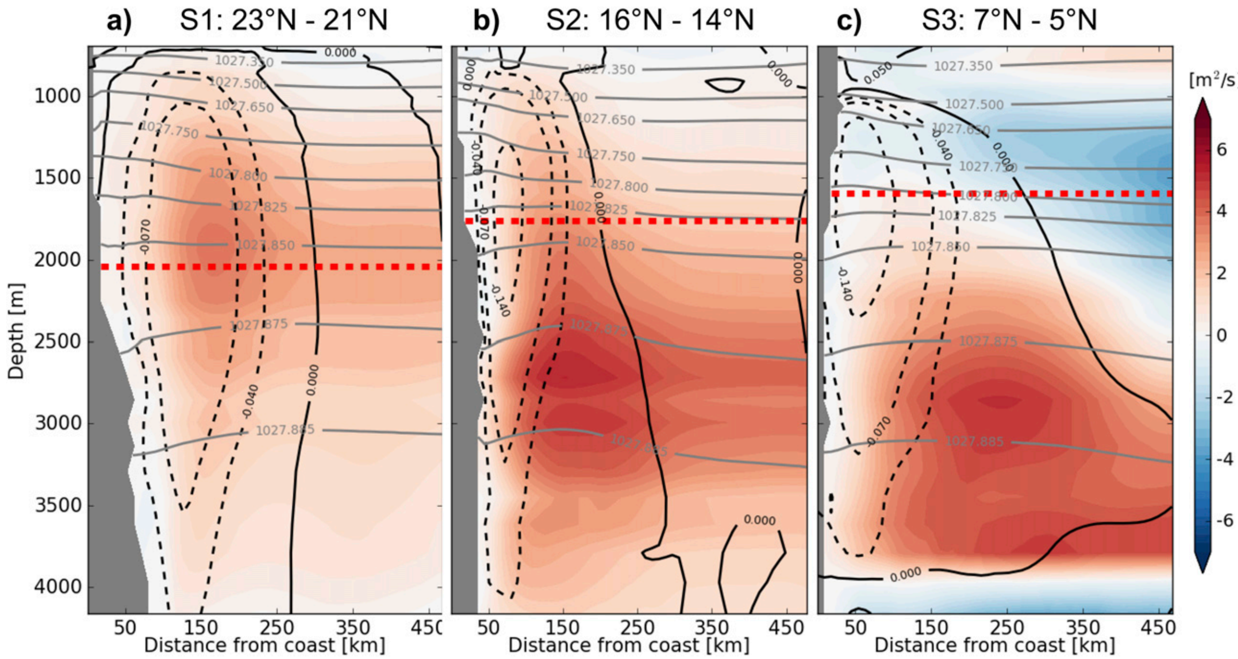

FIG. 11. Pseudozonal overturning per 1 m of shoreline $\tilde{\psi}$ (colors), surface-referenced mean potential density $\overline{\sigma}_0$ (gray contour lines), and along-streamflow $\mathbf{u}_{\parallel}$ (black contour lines, dashed southward) for the three segments north of the equator (a) between 23° and 21°N (S1), (b) between 16° and 14°N (S2), and (c) between 7° and 5°N (S3). Positive (red) $\tilde{\psi}$ indicates clockwise overturning with upwelling close to the shore and downwelling further offshore. The red dashed line marks the DWBC core depth.

because we look at time-averaged quantities. Via Eq. (5), the eddy momentum flux convergence (EMFC) $-\partial\overline{u'_{\perp}u'_{\parallel}}/\partial x_{\perp}$ is a potential driver of the mean across-streamflow $\overline{u}_{\perp}$ and hence for the mean overturning described above (Figs. 11, 12). However, it becomes obvious from Fig. 13, in which we show $-\partial\overline{u'_{\perp}u'_{\parallel}}/\partial x_{\perp}$ for segment S5, that the EMFC cannot serve as an explanation for the overturning normal to the DWBC, which is characterized by a $\overline{u}_{\perp}$ that changes sign in the vertical, with flow toward the shore above the DWBC core and away from the shore below (see Fig. 12b). In case the overturning was related to $-\partial\overline{u'_{\perp}u'_{\parallel}}/\partial x_{\perp}$, this sign change would be reflected in the EMFC. On the contrary, Fig. 13 does not show any significant sign change in the vertical that resembles the scale of the mean overturning visible in Fig. 12b. Instead, the EMFC seems to sharpen the DWBC flow by decelerating it at its edges (positive in Fig. 13, note that the DWBC is directed southward and hence $\overline{u}_{\parallel}$ negative) and accelerating it in its core (negative in Fig. 13). The sharpening of mean currents through EMFC has been described before, predominantly for jet extension flows (e.g., Waterman and Hoskins 2013). We can conclude that the eddy momentum fluxes seem not to play a role for the overturning normal to the DWBC. Instead, the previous analysis suggests that frictional forces are key to the mean overturning. A detailed analysis hereof is beyond the scope of this study. We show the EMFC only for segment S5. However, the picture is very similar in all segments S1–S5. None of them suggests a connection between the EMFC and the overturning normal to the DWBC.

4. Conclusions

We provide a consistent picture of the effect that mesoscale eddies have on the mean density distribution near the deep western boundary current (DWBC) in the Atlantic and the related behavior of the mean flow in the plane normal to the DWBC between 26°N and 20°S. Eddies are crucial in shaping mean density, contributing to leading order to the mean density balance. However, the way they act on density near the DWBC is twofold, revealing an interesting new eddy behavior: *above* the DWBC core depth, eddies *flatten* isopycnals, whereas *below* the core, they *steepen* them, albeit much weaker. This implies that eddies decrease potential energy above the core (in agreement with a GM-like parameterization) and increase potential energy below the core (in contradiction to a GM-like parameterization). It has to be noted that the GM-like eddy effect above the core is considerably stronger then the isopycnal-steepening eddy effect below the core (Figs. 4, 6).

Coarse-resolution ocean models that apply a GM-like eddy parameterization, which exclusively flattens

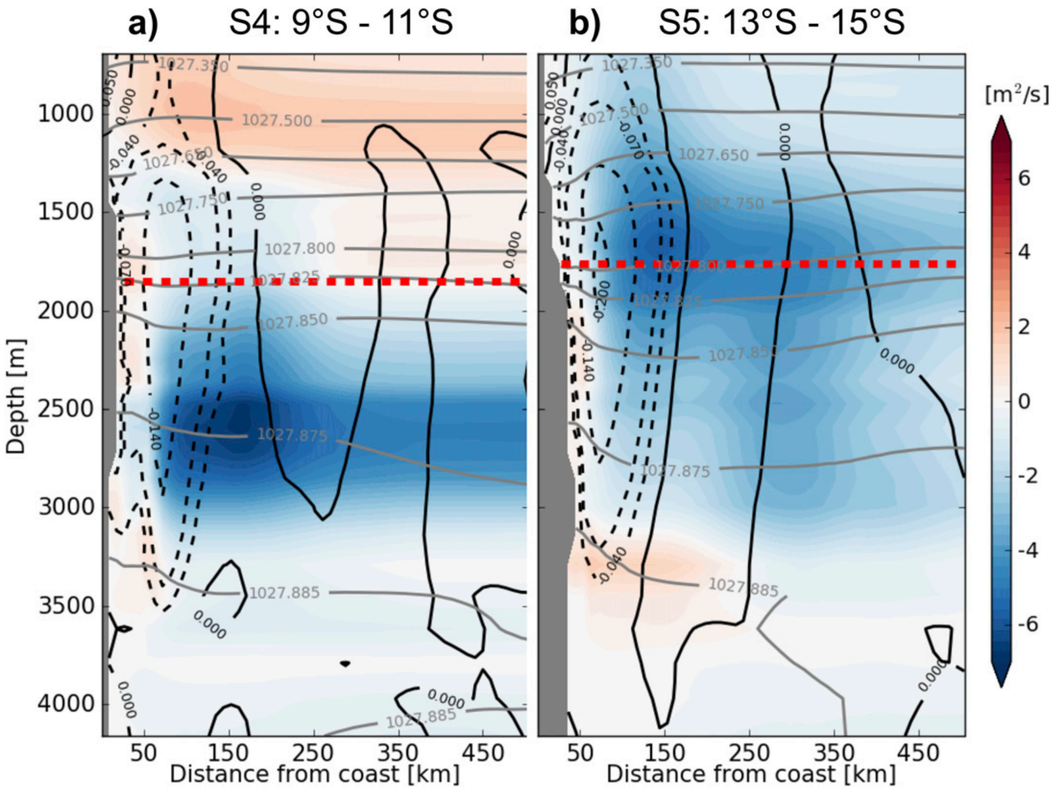

FIG. 12. Pseudozonal overturning per 1 m of shoreline $\tilde{\psi}$ (colors), surface-referenced mean potential density $\overline{\sigma}_0$ (gray contour lines), and along-streamflow $\mathbf{u}_{||}$ (black contour lines, dashed southward) for the two segments south of the equator (a) between 9° and 11°S (S4) and (b) between 13° and 15°S (S5). Positive (red) $\tilde{\psi}$ indicates clockwise overturning. The red dashed line marks the DWBC core depth.

isopycnals, cannot capture the steepening of isopycnals below the DWBC core. Potentially, this leads to a misrepresentation of the true DWBC depth in coarse-resolution ocean models (e.g., Baehr et al. 2004), because the steepening below the core can be interpreted as a downward extension of the DWBC through eddies. A detailed comparison of the DWBC depth in our eddy-resolving STORM simulation and a coarse-resolution version of MPI-OM is planned.

We find evidence for the twofold eddy scenario by analyzing the eddy density flux divergence (EDFD) as well as the pathways of potential energy, which gives us confidence that the described eddy effect is a robust property of the DWBC in our model.

Furthermore, we find that mean density near the DWBC is characterized by a balance between the EDFD and density advection by the mean flow. The eddy-balancing mean advection has the shape of a pseudozonal overturning circulation in the plane normal to the DWBC. In the Northern Hemisphere, we observe a clockwise overturning, with upwelling close to the shore and downwelling further offshore. Consistent with the sign change in the Coriolis parameter, the overturning changes its direction to anticlockwise in the Southern Hemisphere. We could not find any link between the overturning normal to the DWBC and eddy momentum fluxes that was recently established by Li et al. (2016) for an overturning normal to the ACC. Instead, we hypothesize that boundary friction plays a crucial role for the overturning normal to DWBC.

In our analysis, we focus on the Atlantic with its strong DWBC. However, other DWBCs, for example, in the Pacific, might reveal a comparable twofold eddy behavior, because like the DWBC in the Atlantic, they should be characterized by a sign change in the lateral density gradient at the DWBC core depth.

Our analysis is based on geostrophy and therefore does not apply to a narrow band around the equator. However, outside this band, the twofold effect of eddies on density as well as the related pseudozonal overturning are present *everywhere* along the DWBC from 26°N to 20°S. On the one hand, this scenario constitutes a systematic deviation from what is commonly expected from mesoscale eddies. On the other hand, the overturning normal to the DWBC, to the best of our knowledge, was not mentioned in the literature so far and deserves further exploration.

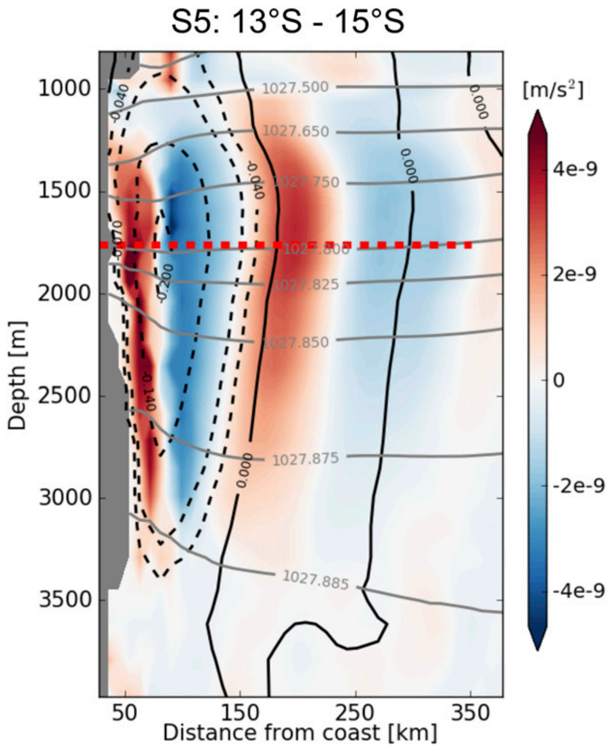

FIG. 13. Across-stream EMFC $-\partial\overline{u'_\perp u'_\parallel}/\partial x_\perp$, surface-referenced mean potential density $\overline{\sigma}_0$ (gray contour lines), and along-streamflow $\mathbf{u}_\parallel$ (black contour lines, dashed southward) for segment S5 from 13° to 15°S. We compute the along-stream/across-stream momentum flux $\overline{u'_\perp u'_\parallel}$ from the model output via $\overline{u'_\perp u'_\parallel} = (1 - 2\sin^2\alpha)\overline{u'v'} + \sin\alpha\cos\alpha(\overline{u'^2} - \overline{v'^2})$, where u and v are the zonal and meridional velocity components and α is the angle between the zonal axis x and the along-stream axis $x_\parallel$. Negative (blue) indicates a deceleration of the southward DWBC through the EMFC. The red dashed line marks the DWBC core depth.

Acknowledgments. We thank Michael Böttinger for providing the 3D-images of the DWBC shown in Fig. 2. Furthermore, we thank Dian Putrasahan and three anonymous reviewers for carefully reading the manuscript and giving valuable comments hereon. Helmuth Haak supported us in all technical concerns. This work was supported by the Max Planck Society and the International Max Planck Research School on Earth System Modelling. We also thank the German consortium project STORM, especially the cluster of excellence CliSAP of the University Hamburg, for making the 0.1° simulation possible.

REFERENCES

Baehr, J., J. Hirschi, J.-O. Beismann, and J. Marotzke, 2004: North Atlantic: A model-based array design study. *J. Mar. Res.*, **62**, 283–312, https://doi.org/10.1357/0022240041446191.

Bower, A. S., M. S. Lozier, S. F. Gary, and C. W. Böning, 2009: Interior pathways of the North Atlantic meridional overturning circulation. *Nature*, **459**, 243–247, https://doi.org/10.1038/nature07979.

Bryden, H., W. Johns, and P. Saunders, 2005a: Deep western boundary current east of Abaco: Mean structure and transport. *J. Mar. Res.*, **63**, 35–57, https://doi.org/10.1357/0022240053693806.

Bryden, H. L., H. R. Longworth, and S. A. Cunningham, 2005b: Slowing of the Atlantic meridional overturning circulation at 25°N. *Nature*, **438**, 655–657, https://doi.org/10.1038/nature04385.

Buckley, M. W., and J. Marshall, 2016: Observations, inferences, and mechanisms of the Atlantic meridional overturning circulation: A review. *Rev. Geophys.*, **54**, 5–63, https://doi.org/10.1002/2015RG000493.

Charney, J. G., 1947: The dynamics of long waves in a baroclinic westerly current. *J. Meteor.*, **4**, 136–162, https://doi.org/10.1175/1520-0469(1947)004<0136:TDOLWI>2.0.CO;2.

Chelton, D. B., M. G. Schlax, R. M. Samelson, and R. A. de Szoeke, 2007: Global observations of large oceanic eddies. *Geophys. Res. Lett.*, **34**, L15606, https://doi.org/10.1029/2007GL030812.

Cunningham, S. A., and Coauthors, 2007: Temporal variability of the Atlantic meridional overturning circulation at 26.5°N. *Science*, **317**, 935–938, https://doi.org/10.1126/science.1141304.

Dengler, M., F. A. Schott, C. Eden, P. Brandt, J. Fischer, and R. J. Zantopp, 2004: Break-up of the Atlantic deep western boundary current into eddies at 8°S. *Nature*, **432**, 1018–1020, https://doi.org/10.1038/nature03134.

Eden, C., R. J. Greatbatch, and J. Willebrand, 2007: A diagnosis of thickness fluxes in an eddy-resolving model. *J. Phys. Oceanogr.*, **37**, 727–742, https://doi.org/10.1175/JPO2987.1.

Fine, R. A., 1995: Tracers, time scales, and the thermohaline circulation: The lower limb in the North Atlantic Ocean. *Rev. Geophys.*, **33**, 1353–1365, https://doi.org/10.1029/95RG00492.

Fischer, J., and F. A. Schott, 2002: Labrador Sea Water tracked by profiling floats—From the boundary current into the open North Atlantic. *J. Phys. Oceanogr.*, **32**, 573–584, https://doi.org/10.1175/1520-0485(2002)032<0573:LSWTBP>2.0.CO;2.

Fox-Kemper, B., R. Ferrari, and J. Pedlosky, 2003: On the indeterminacy of rotational and divergent eddy fluxes. *J. Phys. Oceanogr.*, **33**, 478–483, https://doi.org/10.1175/1520-0485(2003)033<0478:OTIORA>2.0.CO;2.

Garzoli, S. L., S. Dong, R. Fine, C. S. Meinen, R. C. Perez, C. Schmid, E. Van Sebille, and Q. Yao, 2015: The fate of the Deep Western Boundary Current in the South Atlantic. *Deep-Sea Res. I*, **103**, 125–136, https://doi.org/10.1016/j.dsr.2015.05.008.

Gent, P. R., J. Willebrand, T. J. McDougall, and J. C. McWilliams, 1995: Parameterizing eddy-induced tracer transports in ocean circulation models. *J. Phys. Oceanogr.*, **25**, 463–474, https://doi.org/10.1175/1520-0485(1995)025<0463:PEITTI>2.0.CO;2.

Gill, A. E., J. S. Green, and A. J. Simmons, 1974: Energy partition in the large-scale ocean circulation and the production of mid-ocean eddies. *Deep-Sea Res. Oceanogr. Abstr.*, **21**, 499–528, https://doi.org/10.1016/0011-7471(74)90010-2.

Griesel, A., J. L. McClean, S. T. Gille, J. Sprintall, and C. Eden, 2014: Eulerian and Lagrangian isopycnal eddy diffusivities in the Southern Ocean of an eddying model. *J. Phys. Oceanogr.*, **44**, 644–661, https://doi.org/10.1175/JPO-D-13-039.1.

Griffies, S. M., and Coauthors, 2015: Impacts on ocean heat from transient mesoscale eddies in a hierarchy of climate models. *J. Climate*, **28**, 952–977, https://doi.org/10.1175/JCLI-D-14-00353.1.

Jayne, S. R., and J. Marotzke, 2002: The oceanic eddy heat transport. *J. Phys. Oceanogr.*, **32**, 3328–3345, https://doi.org/10.1175/1520-0485(2002)032<3328:TOEHT>2.0.CO;2.

Johns, W., L. Beal, M. Baringer, J. Molina, S. Cunningham, T. Kanzow, and D. Rayner, 2008: Variability of shallow and deep western boundary currents off the Bahamas during 2004–05: Results from the 26°N RAPID–MOC array. *J. Phys. Oceanogr.*, **38**, 605–623, https://doi.org/10.1175/2007JPO3791.1.

Kalnay, E., and Coauthors, 1996: The NCEP/NCAR 40-Year Reanalysis Project. *Bull. Amer. Meteor. Soc.*, **77**, 437–471, https://doi.org/10.1175/1520-0477(1996)077<0437:TNYRP>2.0.CO;2.

Kanzow, T., U. Send, W. Zenk, A. D. Chave, and M. Rhein, 2006: Monitoring the integrated deep meridional flow in the tropical North Atlantic: Long-term performance of a geostrophic array. *Deep-Sea Res. I*, **53**, 528–546, https://doi.org/10.1016/j.dsr.2005.12.007.

——, and Coauthors, 2007: Observed flow compensation associated with the MOC at 26.5°N in the Atlantic. *Science*, **317**, 938–941, https://doi.org/10.1126/science.1141293.

Lee, T. N., W. E. Johns, R. J. Zantopp, and E. R. Fillenbaum, 1996: Moored observations of western boundary current variability and thermohaline circulation at 26.5°N in the subtropical North Atlantic. *J. Phys. Oceanogr.*, **26**, 962–983, https://doi.org/10.1175/1520-0485(1996)026<0962:MOOWBC>2.0.CO;2.

Li, H., and J.-S. von Storch, 2013: On the fluctuating buoyancy fluxes simulated in a OGCM. *J. Phys. Oceanogr.*, **43**, 1270–1287, https://doi.org/10.1175/JPO-D-12-080.1.

Li, Q., S. Lee, and A. Griesel, 2016: Eddy fluxes and jet-scale overturning circulations in the Indo–Western Pacific Southern Ocean. *J. Phys. Oceanogr.*, **46**, 2943–2959, https://doi.org/10.1175/JPO-D-15-0241.1.

Lorenz, E. N., 1955: Available potential energy and the maintenance of the general circulation. *Tellus*, **7**, 157–167, https://doi.org/10.3402/tellusa.v7i2.8796.

Marshall, J., and G. Shutts, 1981: A note on rotational and divergent eddy fluxes. *J. Phys. Oceanogr.*, **11**, 1677–1680, https://doi.org/10.1175/1520-0485(1981)011<1677:ANORAD>2.0.CO;2.

Meinen, C. S., and S. L. Garzoli, 2014: Attribution of Deep Western Boundary Current variability at 26.5°N. *Deep-Sea Res. I*, **90**, 81–90, https://doi.org/10.1016/j.dsr.2014.04.016.

——, M. O. Baringer, and S. L. Garzoli, 2006: Variability in Deep Western Boundary Current transports: Preliminary results from 26.5°N in the Atlantic. *Geophys. Res. Lett.*, **33**, L17610, https://doi.org/10.1029/2006GL026965.

——, W. E. Johns, S. L. Garzoli, E. van Sebille, D. Rayner, T. Kanzow, and M. O. Baringer, 2013: Variability of the Deep Western Boundary Current at 26.5°N during 2004–2009. *Deep-Sea Res. II*, **85**, 154–168, https://doi.org/10.1016/j.dsr2.2012.07.036.

Rhein, M., D. Kieke, and R. Steinfeldt, 2015: Advection of North Atlantic Deep Water from the Labrador Sea to the southern hemisphere. *J. Geophys. Res.*, **120**, 2471–2487, https://doi.org/10.1002/2014JC010605.

Schott, F. A., P. Brandt, M. Hamann, J. Fischer, and L. Stramma, 2002: On the boundary flow off Brazil at 5–10°S and its connection to the interior tropical Atlantic. *Geophys. Res. Lett.*, **29**, 1840, https://doi.org/10.1029/2002GL014786.

——, M. Dengler, R. Zantopp, L. Stramma, J. Fischer, and P. Brandt, 2005: The shallow and deep western boundary circulation of the South Atlantic at 5°–11°S. *J. Phys. Oceanogr.*, **35**, 2031–2053, https://doi.org/10.1175/JPO2813.1.

Sijp, W. P., J. M. Gregory, R. Tailleux, and P. Spence, 2012: The key role of the western boundary in linking the AMOC strength to the north–south pressure gradient. *J. Phys. Oceanogr.*, **42**, 628–643, https://doi.org/10.1175/JPO-D-11-0113.1.

Smeed, D. A., and Coauthors, 2018: The North Atlantic Ocean is in a state of reduced overturning. *Geophys. Res. Lett.*, **45**, 1527–1533, https://doi.org/10.1002/2017GL076350.

Treguier, M., 1999: Evaluating eddy mixing coefficients from eddy-resolving ocean models: A case study. *J. Mar. Res.*, **57**, 89–108, https://doi.org/10.1357/002224099765038571.

Vallis, G. K., 2017: *Atmospheric and Oceanic Fluid Dynamics*. Cambridge University Press, 745 pp.

von Storch, J.-S., C. Eden, I. Fast, H. Haak, D. Hernández-Deckers, E. Maier-Reimer, J. Marotzke, and D. Stammer, 2012: An estimate of the Lorenz energy cycle for the World Ocean based on the STORM/NCEP simulation. *J. Phys. Oceanogr.*, **42**, 2185–2205, https://doi.org/10.1175/JPO-D-12-079.1.

——, H. Haak, E. Hertwig, and I. Fast, 2016: Vertical heat and salt fluxes due to resolved and parameterized meso-scale eddies. *Ocean Modell.*, **108**, 1–19, https://doi.org/10.1016/j.ocemod.2016.10.001.

Waterman, S., and B. J. Hoskins, 2013: Eddy shape, orientation, propagation, and mean flow feedback in western boundary current jets. *J. Phys. Oceanogr.*, **43**, 1666–1690, https://doi.org/10.1175/JPO-D-12-0152.1.

Weatherly, G., Y. Y. Kim, and E. A. Kontar, 2000: Eulerian measurements of the North Atlantic Deep Water deep western boundary current at 18°S. *J. Phys. Oceanogr.*, **30**, 971–986, https://doi.org/10.1175/1520-0485(2000)030<0971:EMOTNA>2.0.CO;2.